



Original Article

# Investigating the elastic modulus and hardness properties of a high entropy alloy coating using nanoindentation



M. Dada <sup>a,\*</sup>, P. Popoola <sup>a</sup>, N. Mathe <sup>b</sup>, S. Adeosun <sup>c</sup>, S. Pityana <sup>a,b</sup>

<sup>a</sup> Chemical, Metallurgical and Materials Engineering, Tshwane University of Technology, Pretoria, South Africa

<sup>b</sup> Council for Scientific and Industrial Research, South Africa

<sup>c</sup> Metallurgical and Materials Engineering, University of Lagos, Akoka, Nigeria

## ARTICLE INFO

### Article history:

Received 2 March 2021

Received in revised form

8 April 2021

Accepted 9 April 2021

Available online 19 April 2021

### Keywords:

Additive manufacturing

High entropy alloys

Nanoindentation

Laser parameters

## ABSTRACT

Using a focused ion beam TTX-NHT3 Nanoindentation tester with a load of 500 mN, we study the micromechanical properties of laser-deposited AlCoCrFeNiCu high entropy alloy coatings. The indentation tests conducted were used to examine the influence of laser power and scan speed on the elastic modulus and hardness of the alloy coatings using the Oliver & Pharr method. There were several indentation points impressed and used to extract the mechanical properties of the alloys, and the results of the alloy were compared with that of the A301 steel substrate. The results showed the mean value of the NanoHardness and Elastic modulus of the high entropy alloy were 2.769 GPa and 149 GPa, respectively. The Vickers hardness showed a 60% decline as the laser power increased from 1200 W to 1600 W. The hardness and the elastic modulus were proportional to each other, both increasing with a decrease in the indentation depth and laser power. The laser-deposited high entropy alloys were more resistant to plastic deformation and had improved mechanical properties than the steel substrate attributed to the solid-solution hardening and lattice distortion effect of the BCC phase structure and aluminium contents, respectively.

© 2021 The Authors. Publishing services by Elsevier B.V. on behalf of KeAi Communications Co. Ltd. This is an open access article under the CC BY-NC-ND license (<http://creativecommons.org/licenses/by-nc-nd/4.0/>).

## 1. Introduction

Materials used for aerospace applications must be lightweight, corrosion-resistant, having good thermal behaviour at elevated temperatures and mechanical features such as toughness, ductility, hardness, creep and strength. Materials used in the aerospace industry with these characteristic features are nickel superalloys, steels, titanium alloys, cobalt-based alloys and more recently high entropy alloys (HEAs) [1].

Yeh et al. [2] reported that high entropy alloys comprise principal elements from the periodic table where the compositional concentration ranges between 5% and 35%, and these elements must at least be five or more for the equilibrium phases in the alloy system to form solid solution phases as opposed to intermetallic compounds [3]. This high entropy effect triggered by an increased

number of elements in the HEAs system causes a lattice distortion attributed to uneven atomic radius by distinct elements in the alloy system [4]. The lattice distortion core effect that hinders the dislocation movement results in excellent hardness and strength, even at elevated temperatures. Diao et al. [5] reported that the Vickers hardness values of HEAs range from 140 HV to 900 HV. However, these values depend on the alloying composition and the manufacturing route. According to Zhang et al. [6], HEAs are fabricated via powder metallurgy, casting, mechanical alloying and additive manufacturing, to mention a few [7]. In the literature, most HEAs are manufactured through arc melting and casting technique, nonetheless, the mechanical properties of as-cast HEAs are generally lower than other manufacturing routes, particularly when compared to materials fabricated via laser additive manufacturing [8,9]. Joseph et al. [10] did a comparative study on HEAs fabricated via arc melting and laser deposition and the authors attributed the variations in both techniques to the difference in thermal gradient and solidification rates [11]. Xiang et al. [12] reported that the laser metal deposition technique (LMD) had better mechanical properties than the as-cast HEAs at cryogenic temperatures and that the LMD allows the adjustments of the mechanical properties of the

\* Corresponding author.

E-mail address: [dadadupeola@gmail.com](mailto:dadadupeola@gmail.com) (M. Dada).

Peer review under responsibility of Editorial Board of International Journal of Lightweight Materials and Manufacture.

HEAs by changing the laser power attributed to the heat flux direction and rapid solidification of the technique. This suggests that the laser parameters have a significant influence on the mechanical properties of laser-deposited HEAs. Sun et al. [13] proposed that the optimization of the laser parameters results in improved mechanical properties and homogeneous microstructures, thus, the importance of studying the effect of these parameters on the mechanical properties of laser-deposited HEAs [14]. Several conventional methods have been used to test the mechanical properties of HEAs, namely; compression, tension and Charpy impact tests [15], however, the lack of in-situ measurements without damaging effects or the demand for standard or bulk sample sizes makes these methods unsuitable [16].

Nanoindentation is a non-destructive technique that provides in-situ indentation measurements on a small area but a wide range of geometries for several materials, including coatings. Thus, avoiding the effect of the substrate at penetration depths as low as 25 nm [17]. This technique uses a Berkovich three-sided pyramid indenter or a four-sided pyramid Vickers indenter. In this study, a Berkovich indenter is used as opposed to a Vickers indenter because the former provides a sharp pointed tip compared to the 0.5 µm slight offset of the Vickers indenter [18]. The Berkovich indenter also probes many points on the surface of the sample through a line, point or grid method [19]. For this reason, this indenter was selected for this study, nonetheless, both Vickers and Berkovich indenters give adequate results accepted by the ISO/FDIS 14577-1 standard [20]. The Nanoindentation technique has been used to examine the creep characteristics [21–23], assessing phase stabilities [24], investigating plastic deformation [25,26], measuring residual stresses [27,28], fracture toughness [29,30], hardness and elastic modulus of polymers, metals and alloys [31–34]. Table 1 shows earlier studies on the nanoindentation of high entropy alloys as having been reported in the literature on thin films via magnetic sputtering [35–39], HEAs via selective laser melting [40–45] or other manufacturing techniques and alloy composition [46]. To our best knowledge, reports on the Nano-indentation of LMD AlCoCrFeNiCu HEA coatings on a steel substrate are limited in the literature. Thus, this study investigates the micro-mechanical properties of LMD AlCoCrFeNiCu HEAs coating by utilizing indentation testing for aerospace applications.

## 2. Material and methods

### 2.1. Laser metal deposition

In this study, the nominal and actual composition of AlCoCrFe-NiCu high entropy alloy powder is shown in Table 2. The

**Table 1**  
Summary of Nanoindentation studies of HEAs.

HEAs	Structure	Property	Process	Substrate	Ref.
AlCoCrFeNiCu	FCC, BCC	Creep, hardness and modulus, fracture toughness and Vickers hardness	LENS	A301 steel	This Study
Al <sub>x</sub> CoCrFeNi	FCC, Disordered BCC and Ordered B2	Hardness and modulus	LENS	CoCrFeNi	[11]
Al <sub>0.5</sub> CoCrFeNi	FCC + BCC	Plastic deformation	Arc Melting	—	[47]
CoCrFeNiMn	FCC and BCC	Hardness and elastic modulus	Magnetron Sputtering	Silicon	[48]
AlCoCuCrFeNiTi	FCC, BCC, Ordered BCC and Tetragonal	Phases, hardness and elastic modulus	Mechanical Alloying	—	[49]
CoCrFeMnNi	FCC	Creep	SLM	—	[40]
FeMnCoCrSiCu	FCC and HCP	Elastoplastic deformation	Casting	—	[26]
AlCrCuFeNi <sub>2</sub>	FCC and BCC	Indentation deformation of the phases	Arc Melting	—	[50]
AlCoCrFeNi	FCC, BCC, Ordered BCC	Pile-up and Sink-in Characteristics	Arc Melting	—	[51]
FeCoNiCrMn and FeCoNiCrMnAl	FCC and FCC + BCC	Elevated temperature creep	Arc Melting	—	[52]

**Table 2**  
Chemical composition of AlCoCrFeNiCu HEA in atomic percentage.

Element	Al (at.%)	Co (at.%)	Cr (at.%)	Fe (at.%)	Ni (at.%)	Cu (at.%)
Nominal	16.6	16.6	16.6	16.6	16.6	16.6
Actual	42.95	11.09	10.24	13.52	10.36	11.84

AlCoCrFeNiCu powder blend used to produce the samples A-E was purchased from FJ Brodmann & CO., LLC each having purity of 99.9%. The as-received powder with particle sizes distribution which ranges from 45 to 106 µm was deposited on a preheated A301 steel substrate of geometric size 10 cm × 5 cm at 400 °C via a laser engineering net shaping (LENS) system at the Council for Scientific and Industrial Research, Pretoria, South Africa and used to fabricate five samples. The LMD process was optimized using the following parameters presented in Table 3, thus, varying the laser power from 1200 to 1600 W and scan speed from 8 mm/s to 12 mm/s while other parameters such as the beam diameter 2 mm, powder feed rate 2 rpm, 50% overlap and 0.5 mm layer thickness on an A301 austenitic steel plate (7% nickel and 17% chromium) remains constant. The microstructure of the alloy was detected using an XPERT-PRO X-ray diffraction system (XRD) and a JEOL-JSM-6101/LA Plus Scanning electron microscope (SEM).

### 2.2. NanoIndentation testing

After deposition, the samples were cut into smaller pieces using a cutting blade machine. The cross-sections of the samples were mounted to expose the surface of the samples for grinding and polishing. The grinding of the surface with grit sizes 80, 320 and 1200 and the polishing to a mirror-finish surface was achieved using Tripoli, intermediates and finishing rouge. The elastic modulus and microhardness were measured on the polished surface of the mounted samples using an Anton-Paar TTX-NHT<sup>3</sup> Nanoindentation tester. The indenter is equipped with a diamond Berkovich three-sided pyramid indenter via the Oliver-Pharr method at the Surface Engineering Research Laboratory (SERL), Pretoria, South Africa.

The equipment shown in Fig. 1 prints an impression in grid form on the surface of the samples through a diamond Berkovich

**Table 3**  
The laser processing parameters.

Sample	A	B	C	D	E
Laser power (W)	1200	1200	1400	1600	1600
Scan speed (mm/s)	8	12	12	10	12

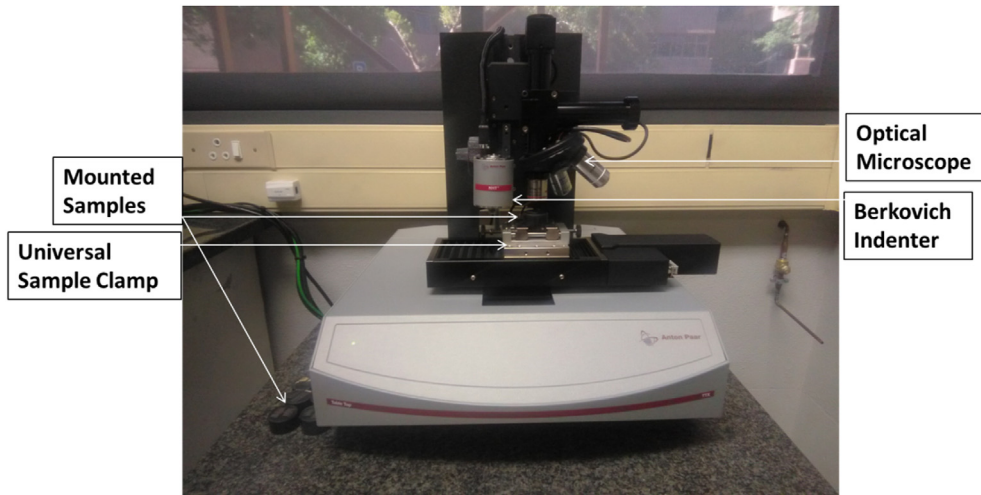


**Fig. 1.** The nanoindentation equipment illustrating the main components.

indenter with an indentation load of 500 mN. The loading and unloading time was placed at 20 s and the holding time between the loading and unloading stage for each test was at 5 s shown in Fig. 2.

### 2.2.1. Nanoindentation theory

The ratio of the peak force  $F_{max}$  to the indentation area  $A_c$  is defined by the hardness and calculated from the equation [53]:

$$H = \frac{F_{max}}{A_c} \quad (1)$$

The area of indentation  $A_c$  is derived from Ref. [53] as:

$$A_c = f(h_c^2) \quad (2)$$

where the contact depth at the peak load is  $h_c$  and can be calculated as in equation [53]:

$$h_c = h_{max} - \epsilon \frac{f_{max}}{S} \quad (3)$$

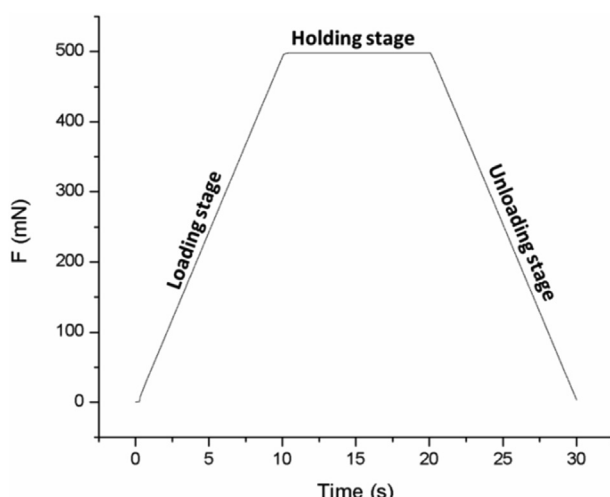


**Fig. 2.** The applied Load- Time Curve.

where the displacement at the maximum load is  $h_{max}$ ,  $S$  is the contact stiffness and  $\epsilon$  is a constant for the indenter geometry at 1.5 for Berkovich indenter [20].

The contact stiffness was calculated using equation (4):

$$S = \left( \frac{dF}{dh} \right)_m = \beta \frac{2}{\sqrt{\pi}} E_r \sqrt{A_c} \quad (4)$$

where  $h$  and  $F$  are the penetration depth and applied load during the indentation tests,  $\beta = 1.034$ , which is the Triangular geometric factor of the diamond shape-dependent indent for a Berkovich indenter [54]. While the reduced modulus  $E_r$  is derived by the equation [55]:

$$\frac{1}{E_r} = \frac{1 - \nu^2}{E} + \frac{1 - \nu_i^2}{E_i} \quad (5)$$

where  $\nu_i$  and  $E_i$  are the elastic modulus and poisons ratio of the indenter and  $E$  and  $\nu$  are the elastic modulus and Poisson's ratio of the samples [56].

The formula by Evans and Wilshaw was used to calculate the fracture toughness ( $K_{IC}$ ) as in Eqs. (6) and (7) [53]:

$$K_{IC} = 0.079 \left( \frac{P}{a^{3/2}} \right) \log \left( 4.5 \cdot \frac{a}{c} \right) \text{ MPa m}^{1/2} \quad (6)$$

$$K_{IC} = \alpha \left( \frac{E}{H} \right)^{0.5} \left( \frac{P}{C^{1.5}} \right) \quad (7)$$

where  $a$  the half indentation is diagonal which is approximately 0.04 for Berkovich indenter [57].  $P$  is the applied normal load,  $c$  is the crack length and half indentation diagonal.

## 3. Results and discussion

### 3.1. The load-displacement curves

Nanoindentation tests were employed to probe the time-dependent nanoscale mechanical properties of the AlCoCrFe-NiCu HEA at room temperature and the microstructural analysis of the alloy was performed using a JEOL-JSM-6010/LA plus scanning electron microscope (SEM) presented in Fig. 3. The

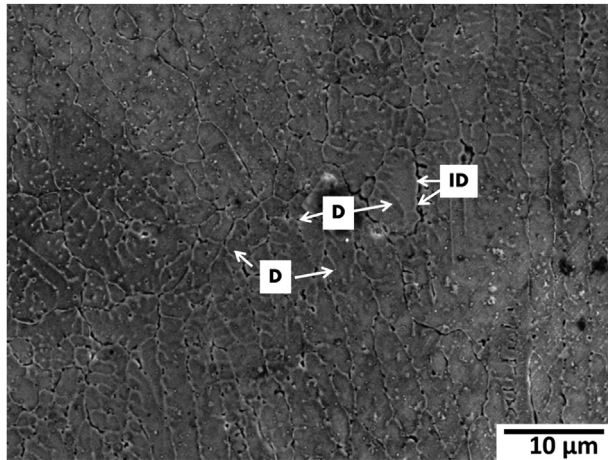


**Fig. 3.** SEM images showing the microstructure of AlCoCrFeNiCu high entropy alloy [68].

changes in laser parameters did not influence the structure of the high entropy alloy produced. Sample A-E exhibited a columnar dendrite BCC phase and a minor FCC phase observed in the interdendritic region made up of Cu. Copper segregated to this region because of its low binding energy and high mixing enthalpy with Ni, Fe, Cr and Co [58–60]. The chemical compositions of the alloy presented in Table 2 show that the actual content of Al is higher than the nominal contents, which acted as a stabilizer for the BCC phase. The structure of the phases was detected using an XPERT-PRO X-ray diffraction system and presented in Fig. 4. The diagram shows the laser-deposited HEA consists of an FCC and BCC phase with or without the changes in laser parameters, signifying that the laser processing parameters did not induce any new phase, however, the structure had dominant BCC phases with the highest intensity at  $44.402^\circ$  and an interplanar distance of  $2.03859 \text{ \AA}$  attributed to Al, which is in agreement with Tang et al. [61]. The solid solution phases observed without traces of intermetallics can be attributed to the high entropy mixing effect. The AlCoCrFeNiCu compositional blend possesses the maximum near equiatomic ratio, solidifying to form solid solution phases [62]. The load-displacement ( $P-h$ ) curves of the samples are shown in Fig. 5 with succession

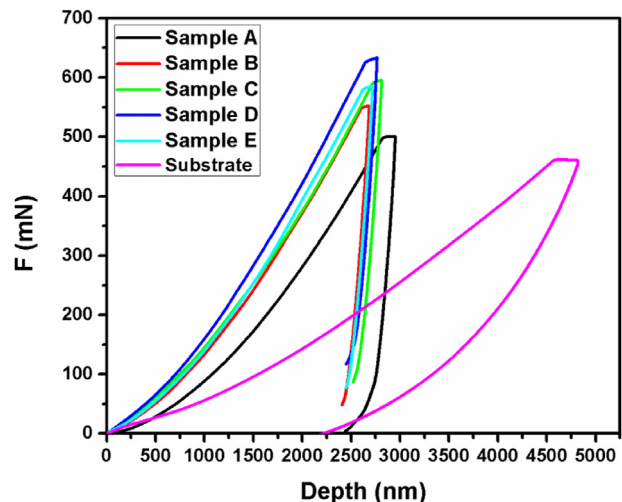


**Fig. 5.** The Nanoindentation force-depth curves of the samples.

loading and unloading stages. Interestingly, the tilt of the A301 steel unloading retract curve showed the baseplate was trying to recover from deformation, however, the indentation depth of the A301 steel substrate was greater than the AlCoCrFeNiCu coatings with a penetration depth of about 2500 nm. Thus, suggesting that the HEA coatings are more resistant to plastic deformation than the steel substrate, attributed to the BCC strengthening phase and the lattice distortion effect of the HEA [63]. Li et al. [64] reported that the plastic deformation for crystalline metals is attributed to the dislocation of slip. Notably, the BCC phase reduces the slipping plane and prevents interplanar dislocations, which stabilizes the microstructure of the alloy and resists plastic deformation [65]. Additionally, plastic deformation is attributed to the movement of the crystal lattice dislocations and the lattice distortion effect of the alloy attributed to the large atomic radius of the elements in the alloy system hinders dislocation movements. It was observed that sample B–E deformed less than sample A due to the low energy input of sample A at high-stress levels. The reduction in the indentation depth influenced an increase in the Nanohardness. Rodriguez et al. [66] also mentioned that the nanoindentation hardness is significantly influenced by the indentation depth, increasing with a decrease in the indentation depth [67].

### 3.2. Modulus and nanohardness

The nominal composition of the laser-deposited high entropy alloys and their respective microstructures were the same; however, the alloys fabricated using several processing parameters resulted in each sample exhibiting different mechanical properties. The elastic modulus and hardness of each sample were calculated by analyzing the load-displacement curves based on the Oliver & Pharr method using a diamond Berkovich indenter with a centerline-to-face angle of  $65.35^\circ$ . The depths of the modulus and hardness were determined using the measurements from the contact stiffness, which is a function of the indentation depth. The results showed the young modulus and hardness were depth-dependent. Therefore, in this depth-sensing indentation test, reduction of the influence of thermal drift on the indentation tests was achieved through machine calibration using fused silica [69]. The modulus responses and the nanohardness had comparable tendencies, decreasing with an increase in the indentation depth [70]. The modulus and hardness of the HEA also showed a 66% and

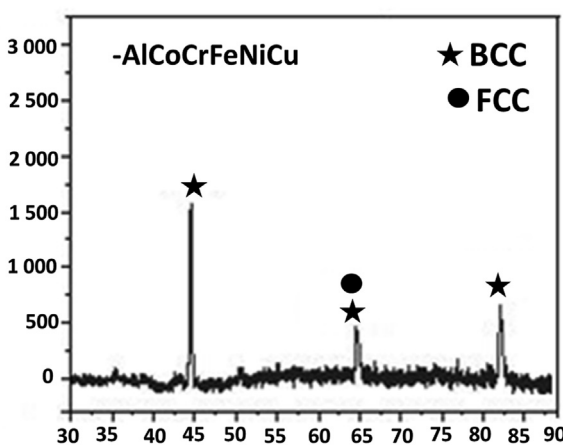


**Fig. 4.** XRD of the AlCoCrFeNiCu high entropy alloy.

60% decrease respectively, as the laser parameters increased from 1200 W to 1600 W with no significant effect from the scanning speed. The data analysis showed that the mean value for the NanoHardness was 2.77 GPa and Elastic modulus 149 GPa, respectively, which were larger than that of the steel substrate (1.2 GPa and 140 GPa, respectively). According to Sun et al. [71], the nanoindentation point arrangement is divided into grid, line and points indentation imprints. The grid nanoindentation method used in this study proved to be effective in conducting the desired Nanoindentation data statistics and getting the mechanical properties of laser-deposited high entropy alloys [72]. Fig. 6 shows the comparison of the mean values of the modulus and hardness of this study with results from the literature. The graph shows that the hardness of sample A to E are in the same range compared with other high entropy alloys, however, the literature [26] showed slightly higher modulus attributed to the variation in the manufacturing process.

### 3.3. Vickers hardness

The average Vickers hardness and the corresponding modulus as a function of the different parameters of the samples and compared with the substrate are plotted in Fig. 7. The Vickers hardness and the nanohardness were proportional to each other for the laser-deposited HEA, the Vickers hardness had a 60% decrease with an increase in laser power from 1200 W to 1600 W. Sun et al. [74] investigated the relationship among Young modulus, indentation hardness and tensile strength of pharmaceutical materials and the authors confirm that the Young modulus is proportional to the hardness for all materials. Nonetheless, the steel substrate showed quite the opposite when comparing the hardness and modulus. The modulus of the substrate showed higher values than the Vickers hardness of the substrate. Generally, the Vickers hardness of the high entropy alloys was 69% higher than the substrate and this is attributed to the BCC phase solid solution strengthening effect of the HEAs. The BCC phase attributed to the high Al content improved the hardness properties [65], in agreement with our previous studies [75]. Thus, the Al element also has one of the largest atomic radii, and the combined increment of the atomic radius in the HEA system resulted in lattice distortion, which also influenced the increment in hardness compared to the steel substrate.

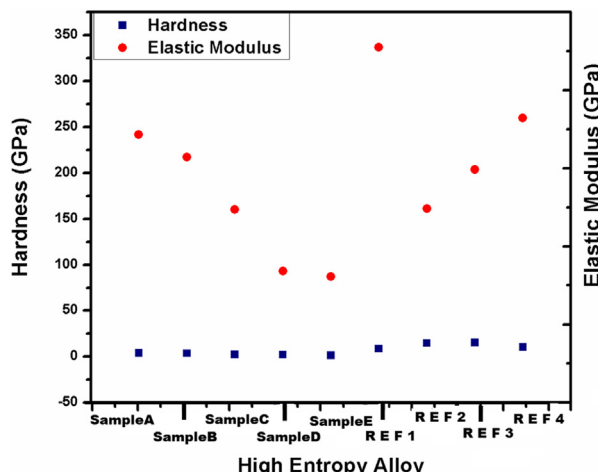


Fig. 6. The comparison of the modulus and nanohardness of present high entropy alloys with the literature [26,49,64,73].

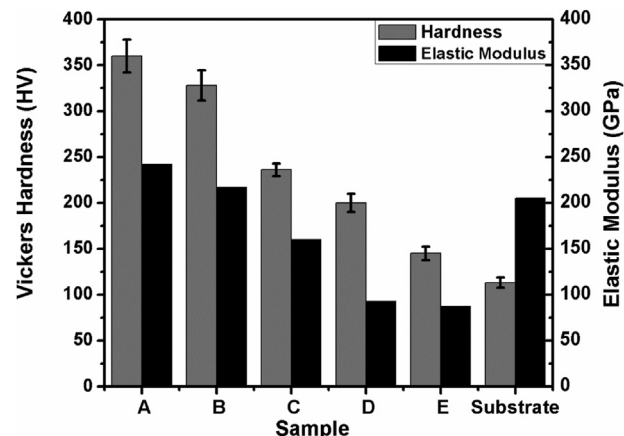


Fig. 7. The Vickers hardness and modulus.

### 3.4. Nanoindentation creep deformation and fracture toughness

The nanoindentation creep time-dependent deformation curves are presented in Fig. 8. As the HEA was stressed at a constant load at room temperature, the number of mobile dislocations reduced and due to the interactions with other dislocations during creep with time, the dislocations were rendered immobile leading to the strain hardening of the alloy since the stress field around the dislocation clusters prevented any dislocation glide. Deformation was further induced when the stress applied increased thus letting the trapped immobile dislocation overcome their restraints and start moving again. The results showed the creep deformation rate of the laser-deposited HEAs was lower than the steel substrate, increasing with an increase in laser power. Moreso, an increase in hardness increased the alloy's capacity to relieve stresses under the applied load. However, the time taken for deformation to occur was relatively close for all samples between 30 and 35 s. Hence, suggesting that a holding time below 30 s suffices to avoid the effect of creep deformation on the unloading curves. Chudoba et al. [76] also proposed a minimum holding time of less than 30 s for high-precision measurements. The deformation was low as the scan speed increases from 8 to 12 mm/s. According to Yu et al. [77], a high scan speed decreases the energy density and reduces the creep of laser-deposited materials, which is due to the increased cooling rate that minimizes the residual stresses.

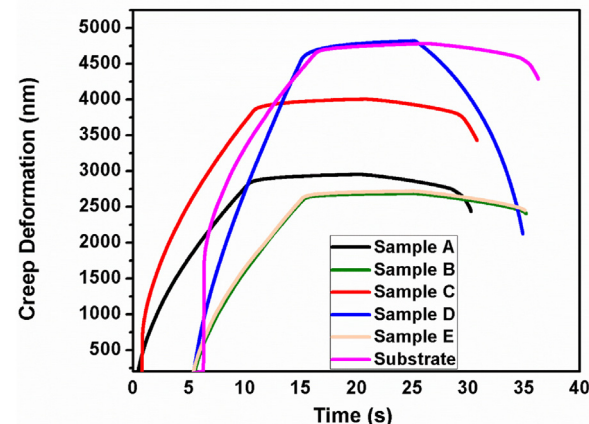


Fig. 8. The Nanoindentation creep deformation-time curve.

The fracture toughness is quantified by the nano-mechanical approach of the samples and characterized as  $K_{IC}$ , by using the ASTM standard E399. As recommended by Li et al. [78], the centerline-to-face angle was about 35.3%. This helped reduce the sample's cracking threshold value. The laser-deposited HEA had greater fracture toughness than the substrate and the fracture toughness decreased with an increase in scan speed at laser power 1200 W and 1600 W, respectively. Sample A and D had fracture toughness of 17.5 MPa m<sup>1/2</sup> and 17.29 MPa m<sup>1/2</sup>, while sample B, C and D had fracture toughness of 14.8 MPa m<sup>1/2</sup>, 12.5 MPa m<sup>1/2</sup> and 15.4 MPa m<sup>1/2</sup>, respectively. Nonetheless, both processing parameters significantly influenced the fracture toughness of the laser-deposited high entropy alloys. All samples were observed not to fail in a brittle manner as the mean fracture toughness values of all samples were more than 10 MPa.

#### 4. Conclusion

The AlCoCrFeNiCu High entropy alloy was fabricated via laser additive manufacturing on an A301 steel substrate, and the micro-mechanical properties of the alloy and its substrate using a nanoindentation tester were investigated. The alloy exhibited both FCC and BCC phases; however, the BCC phase structure was prominent. This phase was responsible for its strength and resistance to plastic deformation compared with the substrate. A reduction in the indentation depth and laser power estimated an increase in the Nanohardness values and modulus and vice versa. The mean value for the NanoHardness was 2.769 GPa, Elastic modulus 149 GPa and fracture toughness was 15.5 MPa m<sup>1/2</sup> under a constant load of 500 mN. The laser processing power had the most influence on the nano-mechanical properties of the laser-deposited high entropy alloy and the alloy had improved mechanical properties than the substrate. This suggests that AlCoCrFeNiCu High entropy alloy can be used as suitable coatings on A301 steel for protection against mechanical failures in aerospace structural applications.

#### Conflicts of interest

The authors declare that there is no conflicts of interest.

#### Acknowledgement

The authors will like to appreciate the Council for Scientific and Research (CSIR), the National Laser Center (Laser Enabled Manufacturing Resource Group) and the Surface Engineering Research Laboratory, Tshwane University of Technology, Pretoria, South Africa for their technical and scientific support during this research.

#### References

- [1] F.C. Campbell Jr., Manufacturing Technology for Aerospace Structural Materials, Elsevier, 2011.
- [2] E.A. Yeh, Nanostructured high-entropy alloys with multiple principal elements: novel alloy design concepts and outcomes, *Adv. Eng. Mater.* 6 (5) (2004) 299–303.
- [3] X. Yin, S. Xu, Properties and preparation of high entropy alloys, in: MATEC Web of Conferences, EDP Sciences, 2018.
- [4] Z. Wang, et al., Effect of lattice distortion on solid solution strengthening of BCC high-entropy alloys, *J. Mater. Sci. Technol.* 34 (2) (2018) 349–354.
- [5] H. Dia, et al., Mechanical properties of high-entropy alloys, *High-Entropy Alloys* (2016) 181–236.
- [6] Y. Zhang, Q. Xing, High Entropy Alloys: Manufacturing Routes, 2020.
- [7] X. Wang, W. Guo, Y. Fu, High-entropy alloys: emerging materials for advanced functional applications, *J. Mater. Chem.* 9 (2) (2021) 663–701.
- [8] C.-M. Lin, H.-L. Tsai, H.-Y. Bor, Effect of aging treatment on microstructure and properties of high-entropy Cu0.5CoCrFeNi alloy, *Intermetallics* 18 (6) (2010) 1244–1250.
- [9] W. Cui, X. Zhang, F. Liou, Additive manufacturing of high-entropy alloys—a review, in: Proceedings of the 28th Annual International Solid Freeform Fabrication Symposium—An Additive Manufacturing Conference, 2017.
- [10] J. Joseph, et al., Comparative study of the microstructures and mechanical properties of direct laser fabricated and arc-melted AlxCoCrFeNi high entropy alloys, *Mater. Sci. Eng.* 633 (2015) 184–193.
- [11] M. Li, et al., Evaluation of microstructure and mechanical property variations in AlxCoCrFeNi high entropy alloys produced by a high-throughput laser deposition method, *Intermetallics* 95 (2018) 110–118.
- [12] S. Xiang, et al., Microstructures and mechanical properties of CrMnFeCoNi high entropy alloys fabricated using laser metal deposition technique, *J. Alloys Compd.* 773 (2019) 387–392.
- [13] K. Sun, et al., Effect of SLM processing parameters on microstructures and mechanical properties of Al0.5CoCrFeNi high entropy alloys, *Metals* 10 (2) (2020) 292.
- [14] S. Xiang, et al., Effects of process parameters on microstructures and tensile properties of laser melting deposited CrMnFeCoNi high entropy alloys, *Mater. Sci. Eng.* 743 (2019) 412–417.
- [15] A. Bhaduri, Mechanical Properties and Working of Metals and Alloys, vol. 264, Springer, 2018.
- [16] F. Pacheco-Torgal, S. Jalali, Nanotechnology: advantages and drawbacks in the field of construction and building materials, *Construct. Build. Mater.* 25 (2) (2011) 582–590.
- [17] W.C. Oliver, G.M. Pharr, An improved technique for determining hardness and elastic modulus using load and displacement sensing indentation experiments, *J. Mater. Res.* 7 (6) (1992) 1564–1583.
- [18] B. Bhushan, B. Gupta, in: R.F. Bunshah (Ed.), Macro And Micro Mechanical and Tribological Properties. Handbook of Hard Coatings—Deposition Technologies, Properties and Applications, Noyes Publications, Park Ridge, New Jersey, USA, 2001, p. 550.
- [19] A.B. Mann, Nanomechanical properties of solid surfaces and thin films. *Nanotribology and Nanomechanics I*, Springer, 2011, pp. 391–437.
- [20] A.R. Franco Jr., et al., The use of a Vickers indenter in depth sensing indentation for measuring elastic modulus and Vickers hardness, *Mater. Res.* 7 (3) (2004) 483–491.
- [21] G. Feng, A. Ngan, Creep and strain burst in indium and aluminium during nanoindentation, *Scripta Mater.* 45 (8) (2001) 971–976.
- [22] S. Soare, et al., Nanoindentation assessment of aluminium metallisation: the effect of creep and pile-up, *Surf. Coating. Technol.* 177 (2004) 497–503.
- [23] D.-H. Lee, et al., Spherical nanoindentation creep behavior of nanocrystalline and coarse-grained CoCrFeMnNi high-entropy alloys, *Acta Mater.* 109 (2016) 314–322.
- [24] V. Maier-Kiener, et al., Nanoindentation testing as a powerful screening tool for assessing phase stability of nanocrystalline high-entropy alloys, *Mater. Des.* 115 (2017) 479–485.
- [25] Z.-M. Jiao, et al., Plastic deformation of Al 0.3 CoCrFeNi and AlCoCrFeNi high-entropy alloys under nanoindentation, *J. Mater. Eng. Perform.* 24 (8) (2015) 3077–3083.
- [26] S. Sinha, et al., Nanoindentation behavior of high entropy alloys with transformation-induced plasticity, *Sci. Rep.* 9 (1) (2019) 1–11.
- [27] L.-N. Zhu, et al., Measurement of residual stresses using nanoindentation method, *Crit. Rev. Solid State Mater. Sci.* 40 (2) (2015) 77–89.
- [28] J. Dean, G. Aldrich-Smith, T. Clyne, Use of nanoindentation to measure residual stresses in surface layers, *Acta Mater.* 59 (7) (2011) 2749–2761.
- [29] D. Harding, W. Oliver, G. Pharr, Cracking during Nanoindentation and its Use in the Measurement of Fracture Toughness, *MRS Online Proceedings Library (OPL)*, 1994, p. 356.
- [30] M. Sebastiani, et al., Measurement of fracture toughness by nanoindentation methods: recent advances and future challenges, *Curr. Opin. Solid State Mater. Sci.* 19 (6) (2015) 324–333.
- [31] G. Fougeres, et al., Young's modulus of nanocrystalline Fe measured by nano-indentation, *Mater. Sci. Eng.* 204 (1–2) (1995) 1–6.
- [32] B.-K. Jang, H. Matsubara, Influence of porosity on hardness and Young's modulus of nanoporous EB-PVD TBCs by nanoindentation, *Mater. Lett.* 59 (27) (2005) 3462–3466.
- [33] R. Wimmer, et al., Longitudinal hardness and Young's modulus of spruce tracheid secondary walls using nanoindentation technique, *Wood Sci. Technol.* 31 (2) (1997) 131–141.
- [34] U. Uyor, et al., Nanomechanical evaluation of poly (vinylidene fluoride) nanocomposites reinforced with hybrid graphene nanoplatelets and titanium dioxide, *Polym. Bull.* (2021) 1–17.
- [35] A.C. Fischer-Cripps, Critical review of analysis and interpretation of nano-indentation test data, *Surf. Coating. Technol.* 200 (14–15) (2006) 4153–4165.
- [36] A. Fischer-Cripps, P. Karvankova, S. Veprek, On the measurement of hardness of super-hard coatings, *Surf. Coating. Technol.* 200 (18–19) (2006) 5645–5654.
- [37] J. Sjölén, et al., Structure and mechanical properties of arc evaporated Ti-Al-O-N thin films, *Surf. Coating. Technol.* 201 (14) (2007) 6392–6403.
- [38] K.E. Raju, et al., The effect of ageing on microstructure and nanoindentation behaviour of dc magnetron sputter deposited nickel rich NiTi films, *Mater. Sci. Eng.* 476 (1–2) (2008) 267–273.
- [39] H.C. Barshilia, et al., Deposition and characterization of TiAlN/TiAlON/Si3N4 tandem absorbers prepared using reactive direct current magnetron sputtering, *Thin Solid Films* 516 (18) (2008) 6071–6078.

- [40] Z. Xu, et al., Microstructure and nanoindentation creep behavior of CoCr-FeMnNi high-entropy alloy fabricated by selective laser melting, *Addit. Manuf.* 28 (2019) 766–771.
- [41] S. Luo, et al., Selective laser melting of dual phase AlCrCuFeNix high entropy alloys: formability, heterogeneous microstructures and deformation mechanisms, *Addit. Manuf.* 31 (2020) 100925.
- [42] R. Zhou, et al., Precipitation behavior of selective laser melted FeCoCrNiCo.05 high entropy alloy, *Intermetallics* 106 (2019) 20–25.
- [43] Y. Wang, et al., Microstructures and properties of equimolar AlCoCrCuFeNi high-entropy alloy additively manufactured by selective laser melting, *Intermetallics* 120 (2020) 106746.
- [44] P. Niu, et al., Microstructures and properties of an equimolar AlCoCrFeNi high entropy alloy printed by selective laser melting, *Intermetallics* 104 (2019) 24–32.
- [45] N.T. Aboulkhair, et al., The microstructure and mechanical properties of selectively laser melted AlSi10Mg: the effect of a conventional T6-like heat treatment, *Mater. Sci. Eng.* 667 (2016) 139–146.
- [46] Y. Zou, Nanomechanical studies of high-entropy alloys, *J. Mater. Res.* 33 (19) (2018) 3035–3054.
- [47] Z. Jiao, et al., Nanoindentation characterised plastic deformation of a Al0.5CoCrFeNi high entropy alloy, *Mater. Sci. Technol.* 31 (10) (2015) 1244–1249.
- [48] C. Dang, et al., Mechanical properties of nanostructured CoCrFeNiMn high-entropy alloy (HEA) coating, *Frontiers in Materials* 5 (2018) 41.
- [49] C. Gómez-Esparza, et al., Microstructural evaluation and nanohardness of an AlCoCuCrFeNiTi high-entropy alloy, *Int. J. Minerals, Metallurgy, and Materials* 26 (5) (2019) 634–641.
- [50] Y. Sun, et al., Nanoindentation deformation of a bi-phase AlCrCuFeNi2 alloy, *J. Alloys Compd.* 608 (2014) 49–53.
- [51] G. Muthupandi, et al., Pile-up and sink-in nanoindentation behaviors in AlCoCrFeNi multi-phase high entropy alloy, *Mater. Sci. Eng.* 696 (2017) 146–154.
- [52] P. Lin, et al., Elevated-temperature creep of high-entropy alloys via nano-indentation, *MRS Bull.* 44 (11) (2019) 860–866.
- [53] M. Masanta, S. Shariff, A.R. Choudhury, Evaluation of modulus of elasticity, nano-hardness and fracture toughness of TiB2–TiC–Al2O3 composite coating developed by SHS and laser cladding, *Mater. Sci. Eng.* 528 (16–17) (2011) 5327–5335.
- [54] H. Attar, et al., Nanoindentation and wear properties of Ti and Ti-TiB composite materials produced by selective laser melting, *Mater. Sci. Eng.* 688 (2017) 20–26.
- [55] A. Hynowska, et al., Nanostructured  $\beta$ -phase Ti–31.0 Fe–9.0 Sn and sub- $\mu\text{m}$  structured Ti–39.3 Nb–13.3 Zr–10.7 Ta alloys for biomedical applications: microstructure benefits on the mechanical and corrosion performances, *Mater. Sci. Eng. C* 32 (8) (2012) 2418–2425.
- [56] Z. Wu, et al., Microstructure characterization of AlxCo1Cr1Cu1Fe1Ni1 ( $x=0$  and 2.5) high-entropy alloy films, *J. Alloys Compd.* 609 (2014) 137–142.
- [57] M. Ayatollahi, A. Karimzadeh, Nano-indentation measurement of fracture toughness of dental enamel, *Int. J. Fract.* 183 (1) (2013) 113–118.
- [58] S. Chen, et al., Temperature effects on the serrated behavior of an Al0.5 CoCrCuFeNi high-entropy alloy, *Mater. Chem. Phys.* 210 (2018) 20–28.
- [59] R. Sriharitha, B. Murty, R.S. Kottada, Phase formation in mechanically alloyed AlxCoCrCuFeNi ( $x=0.45, 1, 2.5, 5$  mol) high entropy alloys, *Intermetallics* 32 (2013) 119–126.
- [60] M. Dada, et al., Process optimization of high entropy alloys by laser additive manufacturing, *Eng. Reports* 2 (10) (2020), e12252.
- [61] Y. Tang, et al., Fabrication and wear behavior analysis on AlCrFeNi high entropy alloy coating under dry sliding and oil lubrication test conditions, *Surf. Rev. Lett.* 23 (4) (2016) 1650018.
- [62] T.M. Yue, et al., Microstructure of laser re-melted AlCoCrCuFeNi high entropy alloy coatings produced by plasma spraying, *Entropy* 15 (7) (2013) 2833–2845.
- [63] C.-C. Tung, et al., On the elemental effect of AlCoCrCuFeNi high-entropy alloy system, *Mater. Lett.* 61 (1) (2007) 1–5.
- [64] J. Li, et al., Atomic-scale analysis of nanoindentation behavior of high-entropy alloy, *J. Micromech. Mol. Phys.* 1 (1) (2016) 1650001.
- [65] S. Guo, C. Ng, C.T. Liu, Anomalous solidification microstructures in Co-free AlxCrCuFeNi2 high-entropy alloys, *J. Alloys Compd.* 557 (2013) 77–81.
- [66] R. Rodriguez, I. Gutierrez, Correlation between nanoindentation and tensile properties: influence of the indentation size effect, *Mater. Sci. Eng.* 361 (1–2) (2003) 377–384.
- [67] V. Kathavate, et al., Analysis of indentation size effect (ISE) in nanoindentation hardness in polycrystalline PMN-PT piezoceramics with different domain configurations, *Ceram. Int.* 47 (9) (2021) 11870–11877.
- [68] M. Dada, et al., The comparative study of the microstructural and corrosion behaviour of laser-deposited high entropy alloys, *J. Alloys Compd.* 866 (2021) 158777.
- [69] G. Feng, A. Ngan, Effects of creep and thermal drift on modulus measurement using depth-sensing indentation, *J. Mater. Res.* 17 (3) (2002) 660–668.
- [70] D. Chen, et al., Nanoindentation experimental study on mechanical properties of as-cast BNi-2 solder alloy, *Procedia Eng.* 130 (2015) 652–661.
- [71] C. Sun, et al., Creep characteristics of coal and rock investigated by nano-indentation, *Int. J. Mining Sci. and Technol.* 30 (6) (2020) 769–776.
- [72] K. Liu, M. Ostadhassan, B. Bubach, Application of nanoindentation to characterize creep behavior of oil shales, *J. Petrol. Sci. Eng.* 167 (2018) 729–736.
- [73] Y. Sun, et al., Local mechanical properties of AlxCrCuFeNi high entropy alloy characterized using nanoindentation, *Intermetallics* 93 (2018) 85–88.
- [74] W.-J. Sun, S. Kothari, C.C. Sun, The relationship among tensile strength, Young's modulus, and indentation hardness of pharmaceutical compacts, *Powder Technol.* 331 (2018) 1–6.
- [75] M. Dada, et al., Effect of laser parameters on the properties of high entropy alloys: a preliminary study, *Mater. Today: Proceedings* 38 (2021) 756–761.
- [76] T. Chudoba, F. Richter, Investigation of creep behaviour under load during indentation experiments and its influence on hardness and modulus results, *Surf. Coatings. Technol.* 148 (2–3) (2001) 191–198.
- [77] J.M. Yu, K.B. Yoon, Investigation of creep behavior of 316L stainless steel produced by selective laser melting with various processing parameters, *J. Mech. Sci. Technol.* 34 (8) (2020) 3249–3259.
- [78] W. Li, P.K. Liaw, Y. Gao, Fracture resistance of high entropy alloys: a review, *Intermetallics* 99 (2018) 69–83.